

This work was written as part of one of the author's official duties as an Employee of the United States Government and is therefore a work of the United States Government. In accordance with 17 U.S.C. 105, no copyright protection is available for such works under U.S. Law.

Public Domain Mark 1.0

<https://creativecommons.org/publicdomain/mark/1.0/>

Access to this work was provided by the University of Maryland, Baltimore County (UMBC) ScholarWorks@UMBC digital repository on the Maryland Shared Open Access (MD-SOAR) platform.

Please provide feedback

Please support the ScholarWorks@UMBC repository by emailing scholarworks-group@umbc.edu and telling us what having access to this work means to you and why it's important to you. Thank you.

Mapping TRMM TMPA into Average Recurrence Interval for Monitoring Extreme Precipitation Events

YAPING ZHOU

Goddard Earth Sciences Technology and Research, Morgan State University, Baltimore, and Earth Sciences Division, NASA Goddard Space Flight Center, Greenbelt, Maryland

WILLIAM K. M. LAU AND GEORGE J. HUFFMAN

Earth Sciences Division, NASA Goddard Space Flight Center, Greenbelt, Maryland

(Manuscript received 29 September 2014, in final form 11 February 2015)

ABSTRACT

A prototype online extreme precipitation monitoring system is developed from the TRMM TMPA near-real-time precipitation product. The system utilizes estimated equivalent average recurrence interval (ARI) for up-to-date precipitation accumulations from the past 1, 2, 3, 5, 7, and 10 days to locate locally severe events. The mapping of precipitation accumulations into ARI is based on local statistics fitted into generalized extreme value (GEV) distribution functions. Initial evaluation shows that the system captures historic extreme precipitation events quite well. The system provides additional rarity information for ongoing precipitation events based on local climatology that could be used by the general public and decision makers for various hazard management applications. Limitations of the TRMM ARI due to short record length and data accuracy are assessed through comparison with long-term high-resolution gauge-based rainfall datasets from the NOAA Climate Prediction Center and the Asian Precipitation–Highly-Resolved Observational Data Integration Toward Evaluation of Water Resources (APHRODITE) project. TMPA-based extreme climatology captures extreme distribution patterns from gauge data, but a strong tendency to overestimate from TMPA over regimes of complex orography exists.

1. Introduction

A number of recent studies have shown increased frequency and intensity of extreme precipitation events in recent decades (Easterling et al. 2000; Trenberth et al. 2003; Groisman et al. 2005; Lau and Wu 2007; Allan and Soden 2008; Min et al. 2011; IPCC 2012). Record-breaking rainfall events have been reported around the world. For example, heavy rain over northern Pakistan in late July 2010 caused the worst flooding in the history of the country. In the spring of 2011, record heavy precipitation events contributed to some of the worst flooding in the lower Mississippi River in the past century. During the same year, North Korea recorded the wettest summer on record since 1908, while heavy monsoon rain caused the worst flooding over Thailand

since 1942. In 2012, Great Britain and Ireland experienced the wettest spring in a hundred years and extensive flooding across the islands. In June 2013, heavy monsoon rain over northern India led to multiple mudslides and 6500 deaths. In September, record-breaking heavy rain in Colorado and subsequent flooding killed eight people and caused \$2 billion in damage. In October, east coast cities of Zhejiang Province in China were submerged in one of the worst flooding on record brought by Typhoon Fitow, with total damage amounting to \$6.7 billion.

Floods are the most widespread and frequent natural disasters caused by extreme rainfall and are responsible for significant loss of lives and property (Smith and Ward 1998; Ashley and Ashley 2008; Grunfest 2009; Adhikari et al. 2010). Floods occur when prolonged rain falls over several days, or intense rain falls over a short period, that exceeds the capacity of the underlying ground or drainage systems, leading to flash floods, overflow of streams, and breach of levees. Heavy rain also has the potential to trigger landslides in

Corresponding author address: Dr. Yaping Zhou, GESTAR/Morgan State University, Climate and Radiation Laboratory, NASA/GSFC, 8800 Greenbelt Rd., Greenbelt, MD 20771.
E-mail: yaping.zhou-1@nasa.gov

mountainous areas with the right combination of topographic slope, soil type, and vegetation. Severe mudslides can be very devastating when they occur in a populated area. For example, a massive rock slide–debris avalanche occurred on 17 February 2006 in the Philippine province of Southern Leyte following a 10-day period of heavy rains. The deadly landslide caused widespread damage with a death toll estimated to be 1126. In August 2009, extreme rain from Typhoon Morakot triggered enormous mudslides and severe flooding throughout southern Taiwan. One mudslide buried the entire town of Xiaolin, killing an estimated 500 people in the village alone.

Tracking and monitoring extreme precipitation globally are very important for climate research as well as hazard management. Recent improvements in satellite-based precipitation retrieval algorithms have made global precipitation measurement and real-time flood and landslide monitoring systems possible. The Tropical Rainfall Measuring Mission (TRMM) Multisatellite Precipitation Analysis (TMPA; Huffman et al. 2007) is one of the more popular satellite-based precipitation estimates utilizing almost all spaceborne precipitation sensors with calibration from TRMM instruments. It combines passive microwave (PMW) precipitation estimates from a variety of low-Earth-orbit satellites, including the TRMM Microwave Imager on TRMM, Special Sensor Microwave Imager (SSM/I) and Special Sensor Microwave Imager/Sounder (SSM/IS) on Defense Meteorological Satellite Program satellites, Advanced Microwave Scanning Radiometer for Earth Observing System (AMSR-E) on *Aqua*, the Advanced Microwave Sounding Unit on the National Oceanic and Atmospheric Administration (NOAA) satellite series, and the Microwave Humidity Sounders on later NOAA-series satellites and the European Operational Meteorological (MetOp) satellite. The microwave precipitation estimates have good physical connections with the hydrometeors above the surface but with a poor space–time coverage. To fill the data gap in the PMW measurements, TMPA merges with PMW-calibrated infrared (IR) products from the international constellation of five geostationary satellites, providing multisatellite precipitation estimates in 3-hourly, $0.25^\circ \times 0.25^\circ$ resolution and quasi-global (50°S – 50°N) coverage. The TMPA estimates are available in the form of two products, a real-time version (3B42-RT) and a gauge-adjusted post-real-time research version (3B42). The research product, which is available 2 months after the end of the month, is recommended for postanalysis. The real-time product, because of its fine resolution and near-real-time availability (available almost 8 h after observation time), has been used in global flood and

landslide monitoring and regional hydrological predictions in many parts of the world (Hossain and Lettenmaier 2006; Hong et al. 2007, 2010; Li et al. 2009; Liao et al. 2010; Yilmaz et al. 2010; Wang et al. 2011; Su et al. 2008, 2011; Wu et al. 2012).

To increase public awareness of extreme precipitation events, it is important that the severity of precipitation events be translated into meaningful terms that can be understood easily by the public and decision makers. “Return period” or “average recurrence interval” (ARI) has been used in the hydrological community to depict the rarity of flood events for decades. An event with ARI of 20 yr means the probability of occurrence in any given year is 1 in 20 or 0.05. This should not be interpreted as only one such event occurring in 20 yr; a 20-yr ARI event in one year does not preclude the same kind of event the next year. The National Weather Service Hydrometeorological Design Studies Center (HDSC) has updated its series of rainfall frequency atlases in terms of ARI (e.g., 100-yr 24-h rainfall depth) in recent years for regions of United States (Bonnin et al. 2011), except for the states in the Northeast and Northwest and Texas. This updated atlas, known as NOAA Atlas 14, not only provided updated information but also established clearer terminology. Near-real-time and prediction maps in ARI are being produced for the contiguous United States (CONUS) from radar and gauge precipitation estimates together with historical ARI statistics from Atlas 14 (<http://metstat.com>; Parzybok et al. 2011). However, since the NOAA atlas is station based, uses point precipitation frequency estimates, and only covers the United States and selected Pacific Islands, near-real-time global precipitation ARI maps are still lacking. A product such as the TRMM near-real-time 3B42RT data is a good candidate to fill the gap in this regard. Obviously, the utility of 3B42RT for climate purposes is still limited because of the short data record. However, the ARI maps combined with available local land-based data can provide much-desired coverage for warning of unusual heavy rain events in many rural areas and developing nations that lack dense surface gauge and radar observations. Additionally, TRMM rainfall ARI maps over the ocean will provide useful scientific information regarding the response of rainfall to climatic fluctuations such as El Niño–Southern Oscillation. As the global rainfall satellite record grows in length from the merging of TRMM and GPM data in the near future, the usefulness of such rainfall ARI maps will become increasingly important for climate change studies.

In this work, we describe extreme-rainfall statistics in the development of an ARI extreme-rainfall warning

system based on 14 yr of TRMM retrospective, version 7, 3B42RT data and conversion of near-real-time TMPA into ARI maps for the region of 50°S–50°N. It is an important value-added TRMM product for research and disaster monitoring purposes, especially for oceanic, remote, or developing regions where surface-based measurement is scarce. In the following sections, we will describe the procedures, results, and limitations of TRMM-based ARI products.

2. Producing ARI maps from TMPA

ARI is computed from frequency analysis of historical precipitation data by fitting the data to predefined distribution functions. There are two basic approaches for extreme value analysis. The first method relies on deriving block maxima (minima) series, frequently chosen as “annual maximum series” in meteorology and hydrology applications. The generalized extreme value distribution (GEV) is often selected to fit the data (Hosking and Wallis 1997; Katz et al. 2002; Wilks 2011). The second method, referred to as the “peak over threshold” (POT), relies on extracting the peak values exceeding a certain threshold from a continuous data record for a given period (Leadbetter et al. 1983; Katz et al. 2002). The number of events and size of exceedances could be fit with the Poisson distribution and the generalized Pareto distribution, respectively. Because extreme precipitation often fits these distribution functions, hydrologists could use them to estimate precipitation with hundreds of return years—many times the length of data record for engineering design (U.S. Department of the Interior Bureau of Reclamation 1987; Koutsoyiannis and Baloutsos 2000). Some studies suggest that the POT method may be better suited for a short data record as it could use more data samples (Coles 2001; Hosking and Wallis 1997; Katz et al. 2002). However, the study of Endreny and Imbeah (2009) showed that GEV distributions could be derived reasonably with only 9 years of TRMM 3B42 data with the assistance of some ground station data for durations larger than 1 day. The HDSC studies found that the best theoretical distribution function for most regions (southern and midwestern states, California, etc.) to represent precipitation extremes was the 3-parameter GEV distribution function (Bonnin et al. 2011; Perica et al. 2013). As a starting point, we will also use the GEV distribution for fitting the AMS from TRMM 3B42RT data and subsequently estimate ARI based on these distributions.

The cumulative distribution function (CDF) of GEV is governed by the following expression:

$$G(x) = \exp \left\langle - \left\{ 1 + \zeta \left[\frac{(x - \mu)}{\sigma} \right] \right\}^{-1/\zeta} \right\rangle, \quad (1a)$$

where $[x: 1 + \zeta(x - \mu)/\sigma > 0]$, and ζ , σ , and μ are the shape, scale, and location parameters respectively. The Gumbel distribution is a special case of the GEV when ζ is zero and the CDF takes the form of

$$G_0(x) = \exp \left\{ - \exp \left[- \left(\frac{x - \mu}{\sigma} \right) \right] \right\}. \quad (1b)$$

The N -yr return value for the GEV distribution (the value that is on average exceeded once in N years) is given by

$$X_N = \mu - \frac{\sigma}{\zeta} \left\{ 1 - \left[- \ln \left(1 - \frac{1}{N} \right) \right]^{-\zeta} \right\}, \quad (2a)$$

and for the Gumbel distribution it is

$$X_{0,N} = \mu - \sigma \ln \left[- \ln \left(1 - \frac{1}{N} \right) \right]. \quad (2b)$$

By fitting the GEV function to observed rainfall data or model outputs, changes in the extremes can be assessed by noting how these shape parameters vary in time or under different climate forcing conditions (e.g., Hosking and Wallis 1997; Huntingford et al. 2003; Schubert et al. 2008). For a given precipitation amount, the GEV facilitates the direct estimation of the ARI by utilizing the precalculated lookup table of precipitation thresholds for different ARIs.

In this study, we first compute the annual maximum (AM) precipitation accumulations from running totals of 1-, 2-, 3-, 5-, 7-, and 10-day time series for all years when 3B42RT data were available (2000–13) for each grid box. Choosing the AM series limits the sample size but is a required procedure for computing the ARI. The three-parameter GEV distributions are derived by fitting the AM series using open source MatLab GEV software (<http://www.mathworks.com/help/toolbox/stats/gevfit.html>), which uses maximum likelihood method to fit the parameters (Kotz and Nadarajah 2000). The best-fit GEV curves and thresholds for 2–100-yr ARI are computed with the derived statistical parameters. As an example, Fig. 1 shows a sample plot of the PDF curves and return thresholds for different accumulation days from a randomly picked single grid point located in the Cascade Range near the border of the states of Washington and Oregon. The PDFs of multiday precipitation accumulation not only shift toward larger values as compared with that of 1-day accumulation as expected, but also show much wider spread with longer tails at high accumulations (Fig. 1a). The tables of the return

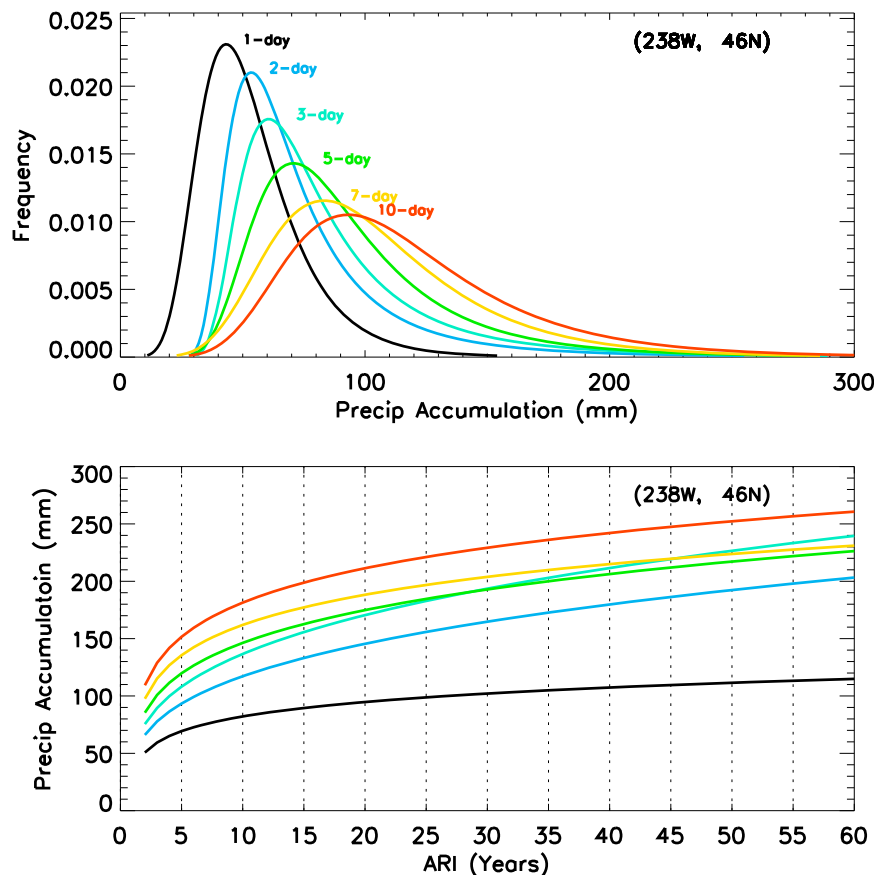


FIG. 1. (top) GEV distributions and (bottom) ARI threshold values derived from TRMM 3B42RT for 1-, 2-, 3-, 5-, 7-, and 10-day precipitation accumulations for a grid box centered on 46.125°N, 238.125°W.

thresholds can be directly used to interpolate the ARI for a given precipitation amount as shown in Fig. 1b. For example, Fig. 1b shows that a daily rainfall of 70 mm or a 10-day accumulation of 170 mm would be qualified as a 10-yr event in this particular location. The near-real-time precipitation accumulations from the past 1, 2, 3, 5, 7, and 10 days are converted into ARI by interpolation. Figure 1b is in fact another form of intensity–duration–frequency (IDF) curve commonly used in the hydrological community where duration and rain depth are plotted for given return year. The IDF curves are used as references for infrastructure design and flood risk assessment. However, because of the short data record and large uncertainty with the TRMM data (discussed in section 3b), we do not recommend using these lookup tables for engineering reference at the present stage. The schematic of the TRMM ARI extreme rain alert system is shown in Fig. 2. The initial plan is to update the ARI maps daily as soon as the latest 3B42RT daily data become available. The statistics and the threshold tables will be updated on a yearly basis when all data from the

previous year become available. For the web application, global maps will show the locations of extreme events with ARI larger than 5 years represented with the largest ARI in the area. Clicking the symbols on the global map can access enhanced regional maps. Figure 3 shows an example of daily precipitation and an ARI map on 27 April 2011. The precipitation map shows areas of heavy precipitation but provides no information on the rarity of these events. The ARI map highlights the areas with locally rare precipitation accumulations that could lead to potential hazards, especially over the lands. For example, a big red dot in the southeastern United States captures the heaviest rain episode with $\text{ARI} > 50\text{yr}$ during the April–May period in 2011. A series of heavy rain events during this period led to massive lower Mississippi River floods—one of the largest and most damaging flooding events recorded along this U.S. waterway in the past century. This product provides additional information of the relative severity of ongoing precipitation events on short and medium time scales that is significant for disaster

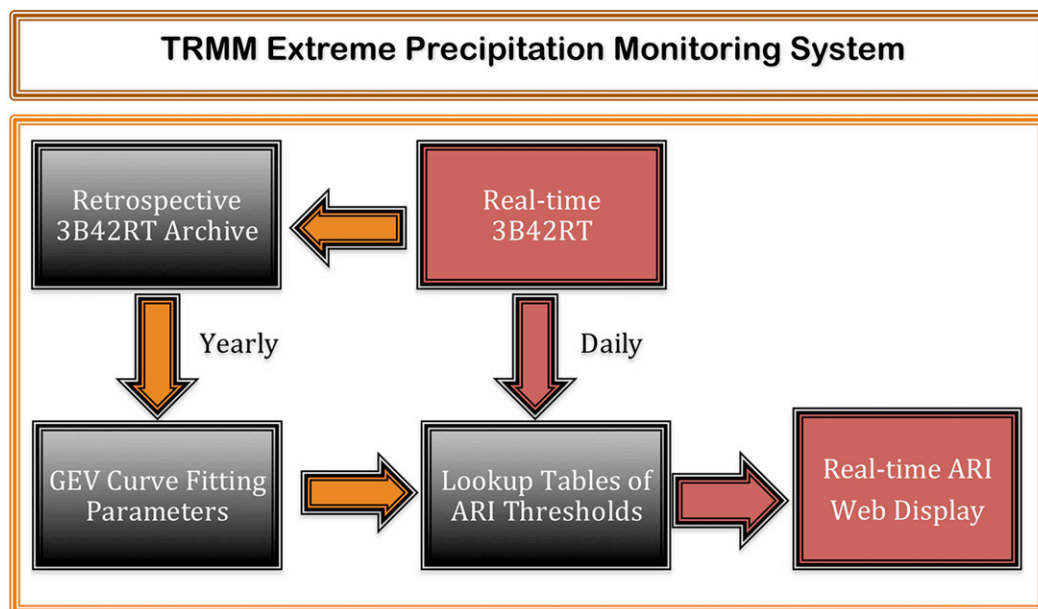


FIG. 2. Schematic of TRMM extreme precipitation monitoring system.

management. Since ARI is location specific and duration dependent, such properties make ARI particularly relevant for public awareness.

3. Results

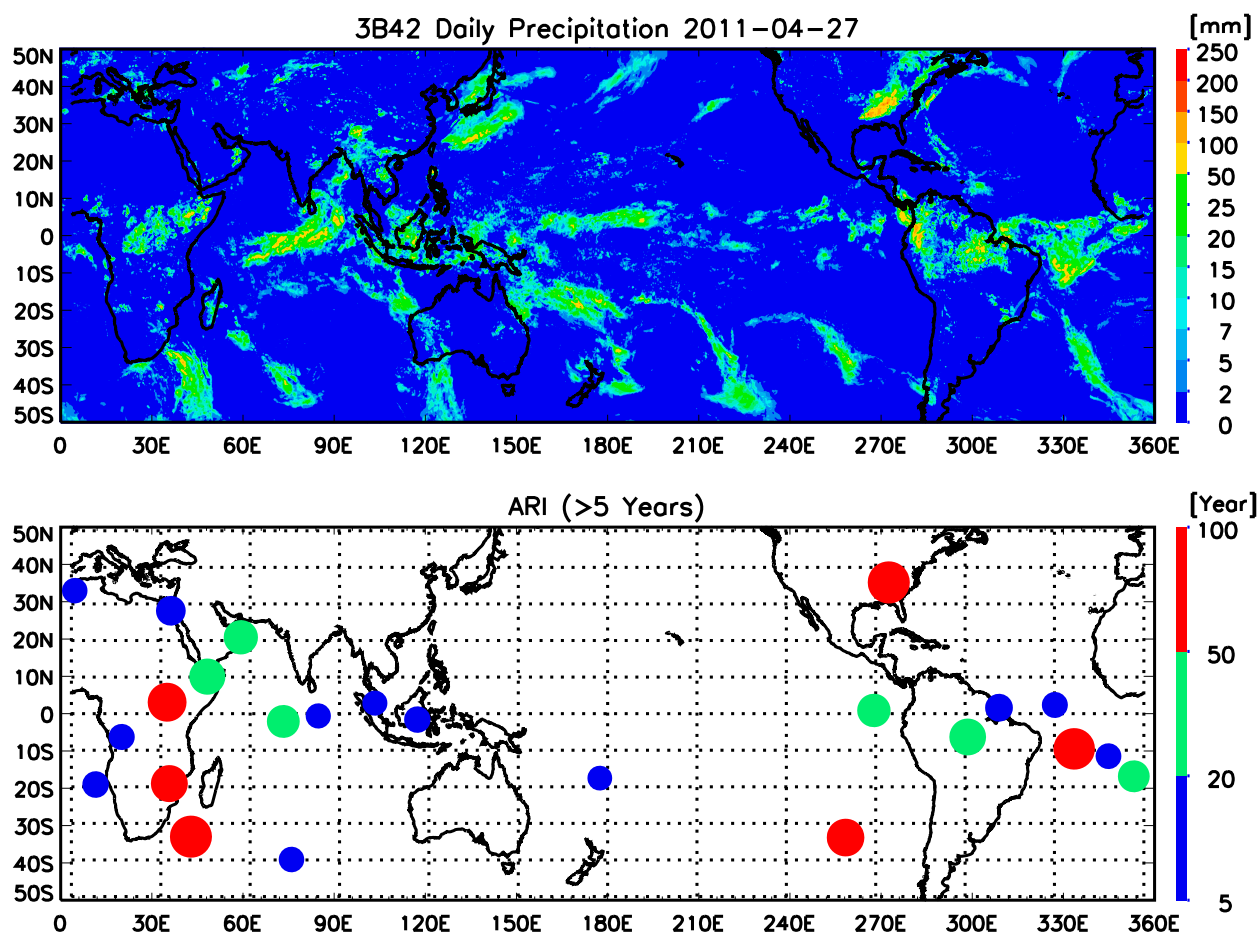
a. ARI depiction of extreme events

To illustrate the capability and the kind of information obtained from an ARI map, we show two recent events that caused much devastation in Southeast Asia. Figure 4 shows an extreme event caused by Typhoon Fitow in October 2013 in the east coast of the Zhejiang Province in China. The map of 3-day precipitation accumulation clearly shows the heavy rain amount along the track of Typhoon Fitow as it made landfall. The related ARI map shows a much smaller region where Fitow dumped over 200 mm of rainfall in three days corresponding to an ARI over 40 yr. The area with high ARI corresponds well with the flooding area in this newly developed wealthy province of China. One measure of the destruction is that an estimate of 75 000 cars in the city of Ningbo alone was submerged. The total loss was estimated to be 5.6 billion U.S. dollars.

One of the major hazards of extreme precipitation is the potential to trigger landslides. A multiday monsoon cloudburst centered over the northern Indian state of Uttarakhand in mid-June 2013 caused devastating floods and landslides in the country's worst natural disaster since the 2004 tsunami. Destruction of bridges and

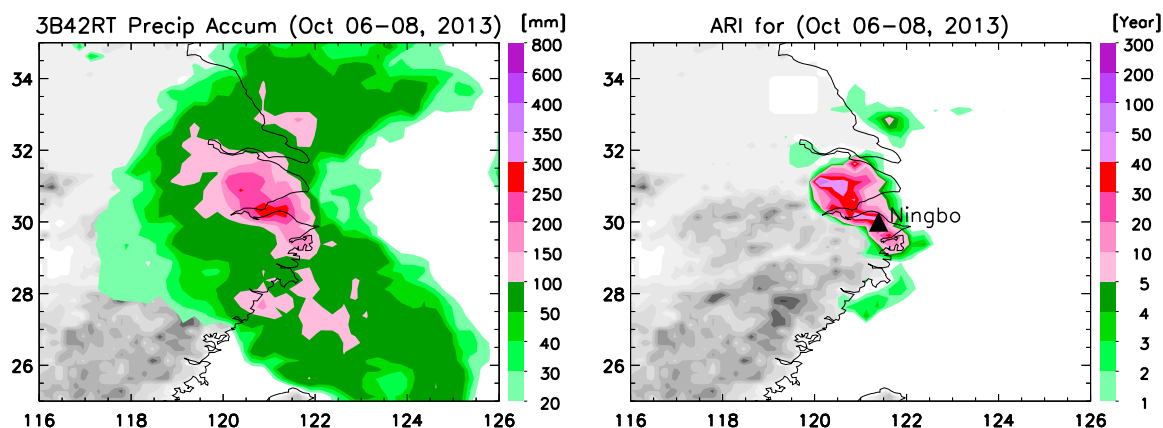
roads left about 100 000 pilgrims and tourists trapped in the valleys leading to three of the four Hindu Chota Char Dham pilgrimage sites, requiring evacuation by Indian military troops. According to figures provided by the Uttarakhand government, more than 5700 people were "presumed dead." Figure 5 shows a large area of heavy 3-day total precipitation accumulation across the Himalaya mountain range near Siwalik from 15 to 17 June with pockets of more than 300-mm total rainfall. The heavy rain caused the melting of Chorabari Glacier at the height of 3800 m and overflow of the Mandakini River, which led to widespread floods downstream. The ARI map highlights regions with elevated ARI with some areas exceeding a 40-yr ARI. Additional ARI maps produced by this approach for major landslide events in recent years can be found in Kirschbaum et al. (2015).

The above examples show that the ARI maps are capable of highlighting regions with particular severity when a large system of extreme precipitation occurs. Severe floods and landslides often occur in areas of elevated ARI or downstream of these areas. Table 1 provides additional examples of some of the most notable and catastrophic flood or landslide events triggered by extreme precipitation since 3B42RT data became available. In each case, the elevated ARI index would provide warning for the ongoing event. We point out that the ARI values depend not only on the actual rain amount but also on the local climatology. For example, a 5-day precipitation accumulation of 100 mm



from Ethiopia counts as a 10-yr event in ARI, yet a 5-day amount of 500 mm in Leyte, Philippines, is only equivalent to a 4-yr event. It is well known that the severity of flood or landslide events is not necessarily proportional

to the magnitude of ARI, as floods and landslides depend on a number of other factors, such as the preceding events, topography, stream distribution, and soil moisture. The actual damage also depends highly on the local



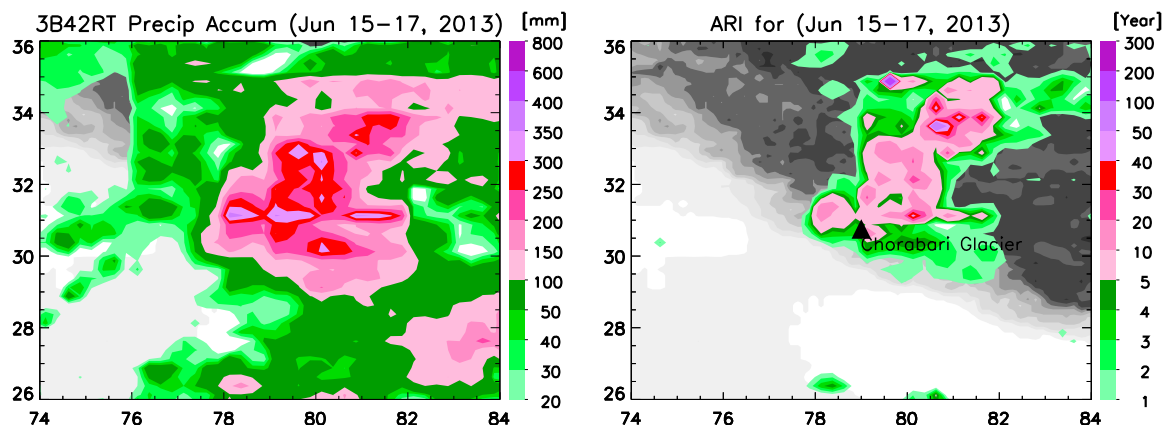


FIG. 5. As in Fig. 4, but during 15–17 Jun 2013 in northern India.

population and development. Nevertheless, ARI maps could provide a near-real-time assessment of the heavy precipitation events that would potentially lead to catastrophic results. The ARI information could be incorporated or serve as supplemental information to locally more sophisticated flood or landslide monitoring system. It could also provide awareness of the going extreme precipitation events around the world for the general public.

b. Limitations of the TRMM ARI

1) GEV STATISTICAL CONFIDENCE

In this section, we will discuss some limitations of the TRMM ARI product due to the accuracy of the real-time 3B42RT data and its short data record. The ARI derived from GEV analysis is expected to be reliable for twice the data length with fitted distribution function (Parzybok et al. 2011); therefore, TRMM data should be able to identify a 28-yr event with reasonable accuracy. However, even though the GEV fitting function allows estimation of events that are outside the range of the current data record, any ARI computed longer than 14 yr (record length) is just extrapolation and subject to high uncertainty. Figure 6 shows examples of fitted GEV functions along with empirical distribution plotted from AM series. The return year (“position”) for the raw data is calculated using a formula based on Gringorten plotting position (Huntingford et al. 2003). This provides a visual inspection of the goodness of fit. The data are generally lining along the fitted black curve. However, the plot for the 3-day accumulation at grid point 20°N, 160°E shows a situation where a single largest value has probably distorted the entire distribution. We also computed the 95% confidence bounds for all the GEV thresholds and found the uncertainty to be

quite large as shown in Fig. 6. The upper bounds depart from the estimated threshold more rapidly with increasing ARI than the lower bounds, which means that the estimated ARI for extreme precipitation could be at the high end of possible range. A normalized 95% confidence range (NCR, defined as the difference of upper bound and lower bound divided by the threshold itself) is computed for all years and all grid points. If the NCR is smaller than 1, the ARI estimates should be within 100% of its magnitude with 95% confidence. Figure 7a shows that for ARI = 5 yr, most of the heavy rain areas—that is, the ITCZ, Asian monsoon, and Amazon regions—have reasonable estimates of ARI as indicated by $NCR < 1$. Low confidences ($NCR > 2$) are observed in dry regions such as North Africa, the Arabian deserts, and the southeast Pacific. The confidence deteriorates dramatically when ARI reaches 20 yr, as shown in Fig. 7b, with $NCR > 1$ covering most of the globe except the ITCZ region. The poor confidence is mainly due to short record length, and partly owing to the statistical methods used to derive the ARI not optimized for the current data record (Katz et al. 2002; Hosking and Wallis 1997). As the data record of merged TRMM–GPM rain data grows in length, the confidence of high ARI will increase.

It should be pointed out that a climatological GEV distribution assumes the stationarity of the data; that is, there is no systematic change in the data record and no such changes will occur. Several studies have reported nonstationarity of precipitation records in some regions during the last half-century (Towler et al. 2010; Cheng et al. 2014). Because of the short record of the TRMM data, nonstationarity is not considered at the present; however, this does not imply that the TRMM data do not present any measurable trend in the extreme precipitation. Nonstationarity should be considered in

TABLE 1. Example extreme precipitation events in the TMPA real-time (RT) data period. The total rain amount is computed from 3B42RT data; measurements for the same duration from other datasets are in parentheses. Numbers in parentheses after return years are number of grid boxes that exceed the given return year. Damage could include destruction from other related causes, such as wind, storm surge, and preceding and subsequent close-by events. Except for the first three floods that occurred in recent years in the United States, all the other floods can be found in http://en.wikipedia.org/wiki/List_of_deadliest_floods.

Date	Location	Rain amount	Return year	Cause	Damage
7–13 Sep 2013	Colorado	85 mm/7 days (180 mm, CPC; 85 mm, 3B42)	5(5) (340, CPC; 300, 3B42)	Heavy rain	8 deaths, \$2 billion in damage
28–29 Oct 2012	New Jersey	260 mm/2 days (160 mm, CPC; 200 mm, 3B42)	50(7) (5, CPC; 20, 3B42)	Tropical Cyclone Sandy	\$65 billion damage
23–27 Apr 2011	Mississippi Valley	450 mm/5 day (300 mm, CPC; 320 mm, 3B42)	100(3) (250, CPC; 75, 3B42)	Heavy rain	>400 deaths, \$2–4 billion damage
27–29 Jul 2010	Pakistan	170 mm/3 days (280 mm, 3B42)	20(4) 90(4)	Heavy monsoon rain	~2000 deaths
7–9 Aug 2009	Taiwan	550 mm/3 days (600 mm, 3B42)	40(7) 50(5)	Typhoon Morakot	677 deaths
8–14 Aug 2007	North Korea	400 mm/7 days (500 mm, 3B42)	40(16) 60(16)	Heavy rain	610 deaths
26 Aug–2 Sep 2006	Ethiopia	150 mm/7 days (140 mm, 3B42)	10(2) 10(2)	Heavy rain	705 deaths
6–12 Feb 2006	Leyte, Philippines	500 mm/5 day (520 mm, 3B42)	4(3) 15(9)	Storm	>1500 deaths
1–3 Sep 2005	Anhui, China	260 mm/3 day (420 mm, 3B42)	50(5) 70(5)	Rain storms	Affected 210 000 people, flattened 10 000 houses
5–11 Jul 2004	Eastern India	1100 mm/7 days (1150 mm, 3B42)	60(5) 70(5)	Monsoon rain	3076 deaths

future studies when the TRMM–GPM data record becomes longer (Katz 2010; Gilleland and Katz 2014, manuscript submitted to *J. Stat. Software*).

2) COMPARISON OF TRMM EXTREME CLIMATOLOGY WITH GAUGE-BASED OBSERVATIONS

Another aspect of the uncertainty comes from the data quality. The real-time 3B42RT data still have many issues regarding data accuracy, especially when extreme events are considered (AghaKouchak et al. 2011; Sorooshian et al. 2011). Even though the TMPA real-time and research product systems are designed to be as similar as possible to ensure consistency between the resulting datasets, it is generally expected that the research version of TMPA has better quality than the real-time version over the land because of its monthly gauge adjustment and calibration by TRMM Combined Instrument estimates (Huffman et al. 2010). The 3B42 and 3B42RT data have been evaluated extensively in recent years with surface radar and gauge-based measurements in multiple spatiotemporal scales over CONUS and many other parts of the world (e.g., Tian et al. 2007, 2009; Ebert et al. 2007; Habib et al. 2009; Villarini and Krajewski 2007; Shen et al. 2010; Villarini 2010; AghaKouchak et al. 2011; Stampoulis and Anagnostou 2012). In general, satellite retrievals can capture heavy rain events over warm seasons and heavy rainfall resulted from tropical convective system, but the quantitative estimates tend to deteriorate as the heavy rain thresholds increase (Mehran and AghaKouchak 2014). For example, Habib et al. (2009) compared 3B42 and 3B42RT data with ground gauge and radar observations during six tropical-related heavy rainfall events over Louisiana, and found the bias of 3B42 and 3B42RT data within $\pm 25\%$ and $\pm 50\%$ at their native temporal and spatial scales, respectively. Chen et al. (2013) compared several satellite rainfall algorithms with surface rain gauge measurements during super Typhoon Morakot on Taiwan Island in August 2009. The 3B42RT was found to underestimate rainfall by 19% compared to gauge measurements even though it had the lowest bias among the four satellite algorithms compared. It is understood that extreme precipitation remains one of the main uncertainties in satellite precipitation retrieval and more detailed evaluations are needed to assess the quality and error characteristics of these datasets in a variety of different geographical regions and for different precipitation systems (Sorooshian et al. 2011).

Here, we evaluate the TRMM ARI product in two steps. The first step is to compare the GEV statistics from 3B42RT with those from independent high-quality long-term observations with similar spatial and

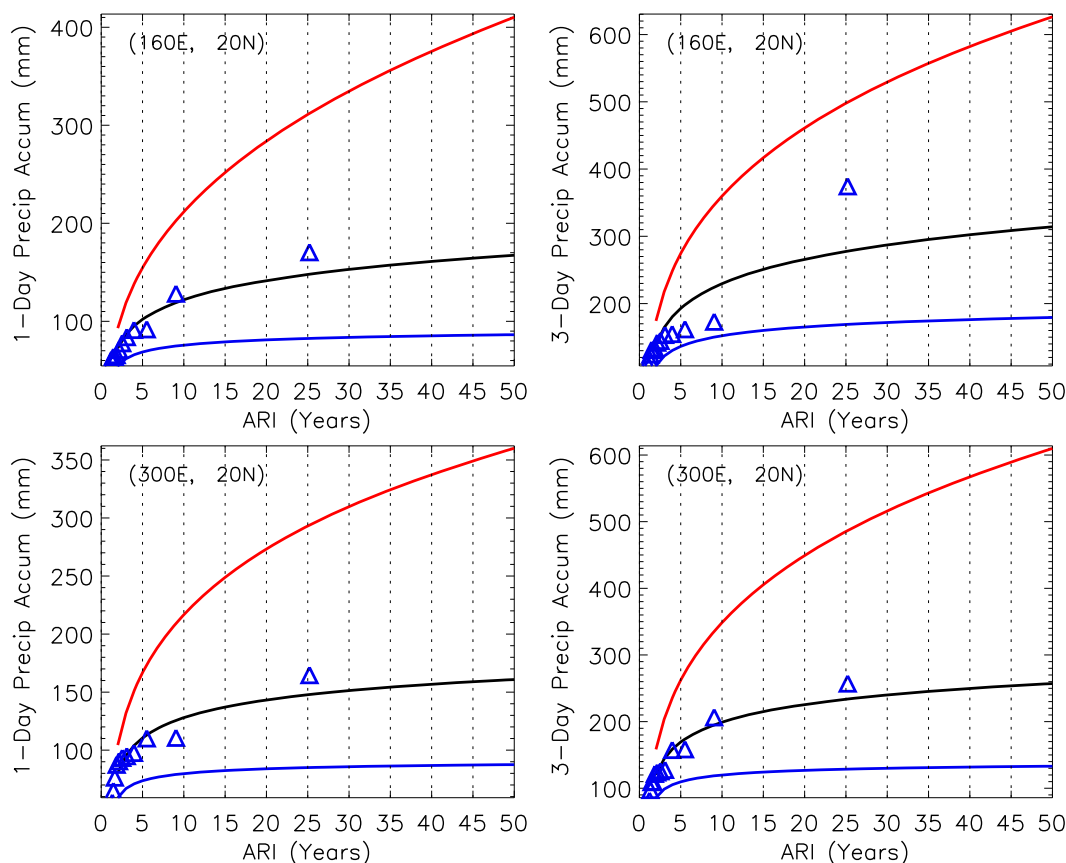


FIG. 6. ARI thresholds and the 95% confidence bounds (mm) for (left) 1- and (right) 3-day precipitation accumulations at grid points centered at (top) 20.125°N, 160.125°E and (bottom) 20°N, 300.125°E. The triangles mark the observed annual maximum precipitation from the period 2000–13.

temporal resolutions, and the second step is to evaluate the derived ARI for the actual events. Long-term high-resolution precipitation datasets have only become available in recent years even for gauge-based observations. We used two such datasets that meet these criteria: one is the NOAA's Climate Prediction Center (CPC) daily U.S. unified precipitation datasets (Higgins et al. 2000). The CPC daily unified precipitation dataset (1948–2012) is a gauge-based, gridded, and quality-controlled product derived from daily and hourly precipitation measurements from over 13 000 (8000 before 1992) stations over CONUS with the same 0.25° spatial resolution as the 3B42 and 3B42RT data. The other dataset comes from the Asian Precipitation–Highly-Resolved Observational Data Integration Toward Evaluation of Water Resources (APHRODITE) project (Yatagai et al. 2012). APHRODITE has produced high-resolution quality-controlled daily gridded precipitation datasets based on data collected at 5000–12 000 stations covering the Asian monsoon region over the Himalayas, Southeast Asia, and mountainous

regions of the Middle East for the years 1957–2007. This study used their 0.25° products for the Asian monsoon and Middle East regions.

The GEV statistics of extreme precipitation from different datasets can be compared using return thresholds regardless of record length. Figure 8 shows the 5-yr thresholds for 3-day precipitation accumulations from 3B42RT and those from CPC over CONUS, and APHRODITE over Asian monsoon and Middle East regions. Over CONUS, the 3B42RT displays similar patterns of geographical distributions of the required rainfall thresholds, which resemble the geographical distributions of the annual mean precipitation. It shows larger thresholds in the eastern half of CONUS east of 102°W, the Pacific Northwest, and Sierra Nevada range, and lower thresholds in the desert Southwest, Great Basin, valleys of northeast Arizona, eastern Utah, central Wyoming, and the Willamette Valley. The 3B42RT misses heavy rain along the Pacific Northwest and Sierra Nevada because of its poor performance in complex orographic regions (Huffman et al.

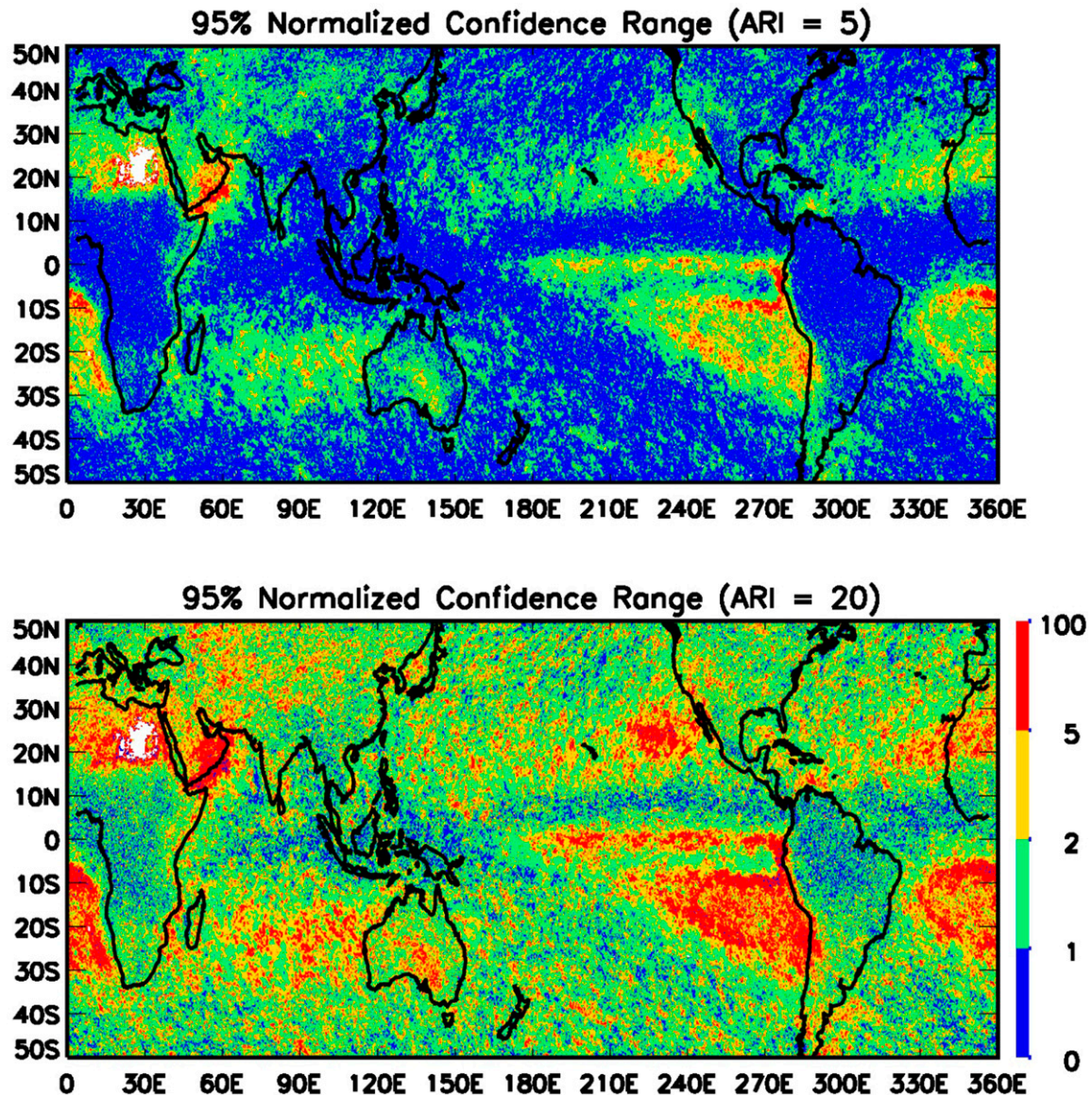


FIG. 7. Normalized 95% confidence range (see definition in the text) for 3-day precipitation accumulations for ARI of (top) 5 and (bottom) 20 yr. The scale is nondimensional.

2010). The 3B42RT shows similarly low precipitation thresholds for most of the desert Middle East with slightly higher values surrounding the Black Sea. Over the Asian monsoon region, there is general overestimation of extreme precipitation, especially over the highlands in middle India, Tibet, and Southeast Asia, which has been reported in previous studies (Shen et al. 2010). The overestimation of extreme precipitation over tropical Pacific islands is noteworthy. On the other hand, it is also likely that APHRODITE underestimates precipitation because of limited gauge number and grid average. Low estimates, especially for extreme precipitation, are likely to occur when the grids have fewer

than two gauge stations (P. Xie 2014, personal communication). These results emphasize the utility of converting different datasets in ARI.

To understand how the length of data record and the data quality affect the results, we further compared ARI thresholds computed from 3B42RT with the following datasets: version 7 of the 3B42 data (1998–2012) and a subset (1998–2012) and full length (1948–2012) of the CPC unified dataset (Fig. 9). The CPC data with full record length (1948–2012), which are considered to provide the best statistics, show a much smoother distribution than the same data with a short record length (1998–2012). The impact of record length is more

20-Year RV (3-Day Accum)

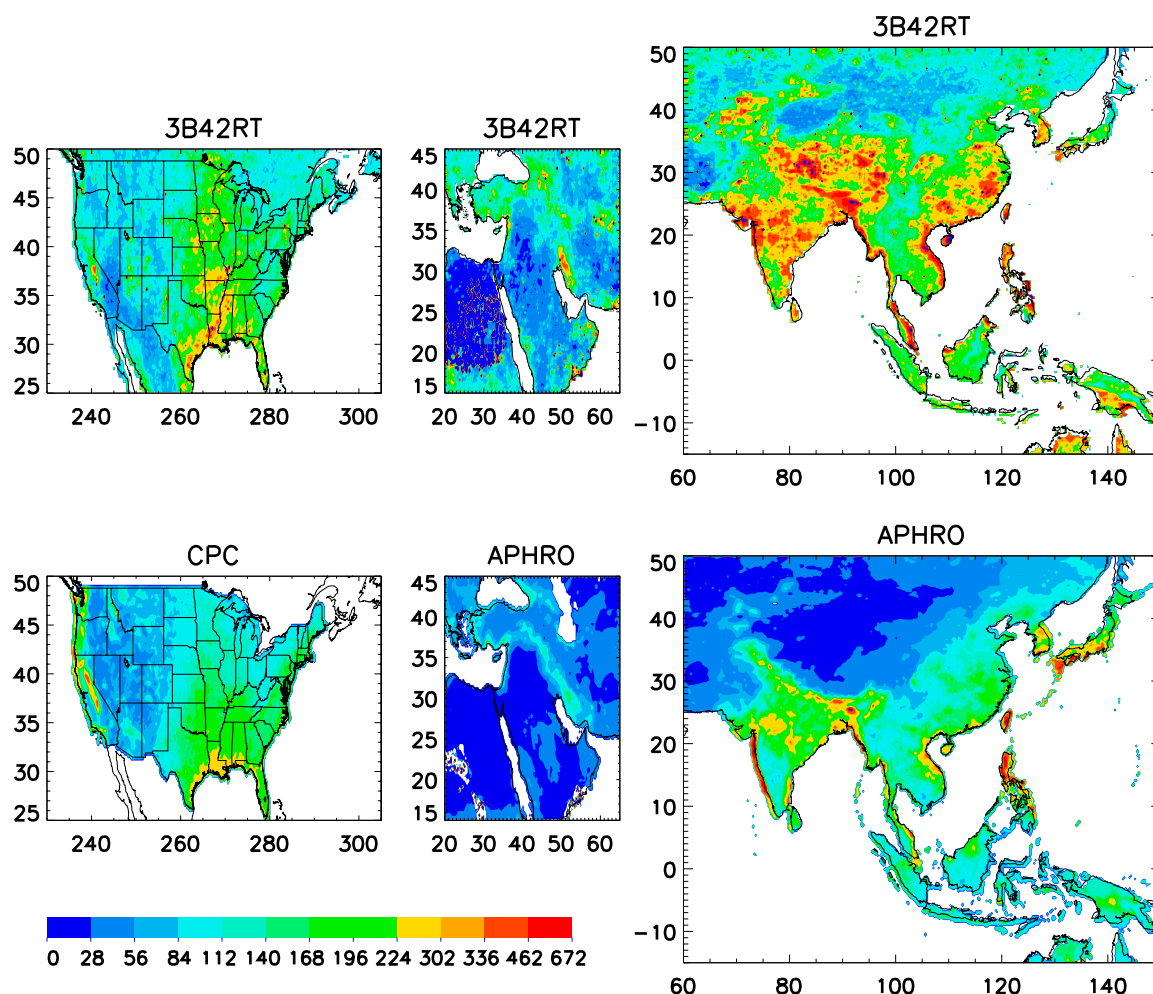


FIG. 8. ARI threshold maps of 20 yr for 3-day precipitation accumulations (mm) from (top) 3B42RT and (bottom left) CPC data, (bottom middle) APHRODITE Middle East, and (bottom right) APHRODITE Asian monsoon datasets.

pronounced with higher ARI values, as the thresholds for the 25-yr ARI are more sporadic than that for the 2-yr ARI in the CPC short-length data. This indicates that inadequate record length in the short data may produce some unreasonably large values in some areas. The sporadic large values in the lower Mississippi River could be caused by a few large events in the short CPC data record. When compared with the CPC data, the 3B42 and 3B42RT data show a much larger area of heavy rain from the Gulf Coast extending farther north to the north-central United States. The overestimation of precipitation by the TMPA in the north-central United States is probably due to its microwave retrieval algorithm based solely on scattering signals of solid hydrometeors. While the 3B42RT misses heavy rain along the Pacific Northwest and Sierra Nevada as

mentioned earlier, the adjustment to the monthly gauge measurements in the 3B42 has likely led to its overestimation of individual rain events along the East Coast and Pacific Northwest.

Since some of the biases in 3B42RT are systematic because of the intrinsic limitations of the retrieval algorithm, these biases are built into the background statistics and the ARI thresholds using the retrospective 3B42RT data. Figure 10 shows an example of computed ARI maps using the full-length CPC data (1948–2012) and 3B42RT data, respectively, for the extreme rain event in the central United States during 23–27 April 2011. The storm was the heaviest among several heavy rain episodes during the April–May period that led to massive lower Mississippi River floods in 2011. The 3B42RT data capture remarkably well the magnitude

1-Day Accumulation

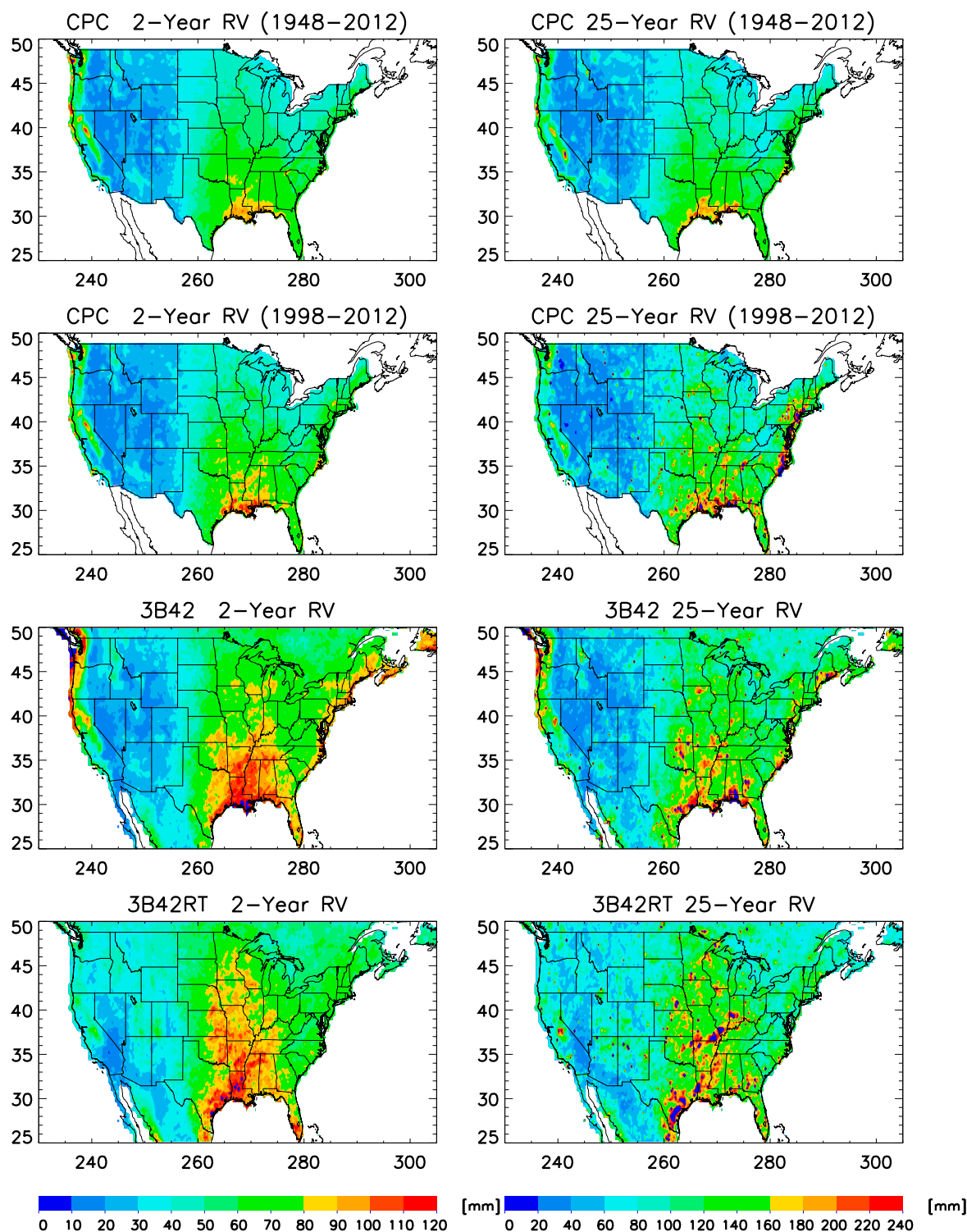


FIG. 9. ARI threshold maps (mm) of (left) 2 and (right) 25 yr for CPC unified daily data for the periods 1948–2012 and 1998–2012, 3B42 (1998–2012), and 3B42RT (2000–13) for 1-day precipitation accumulation for the CONUS area.

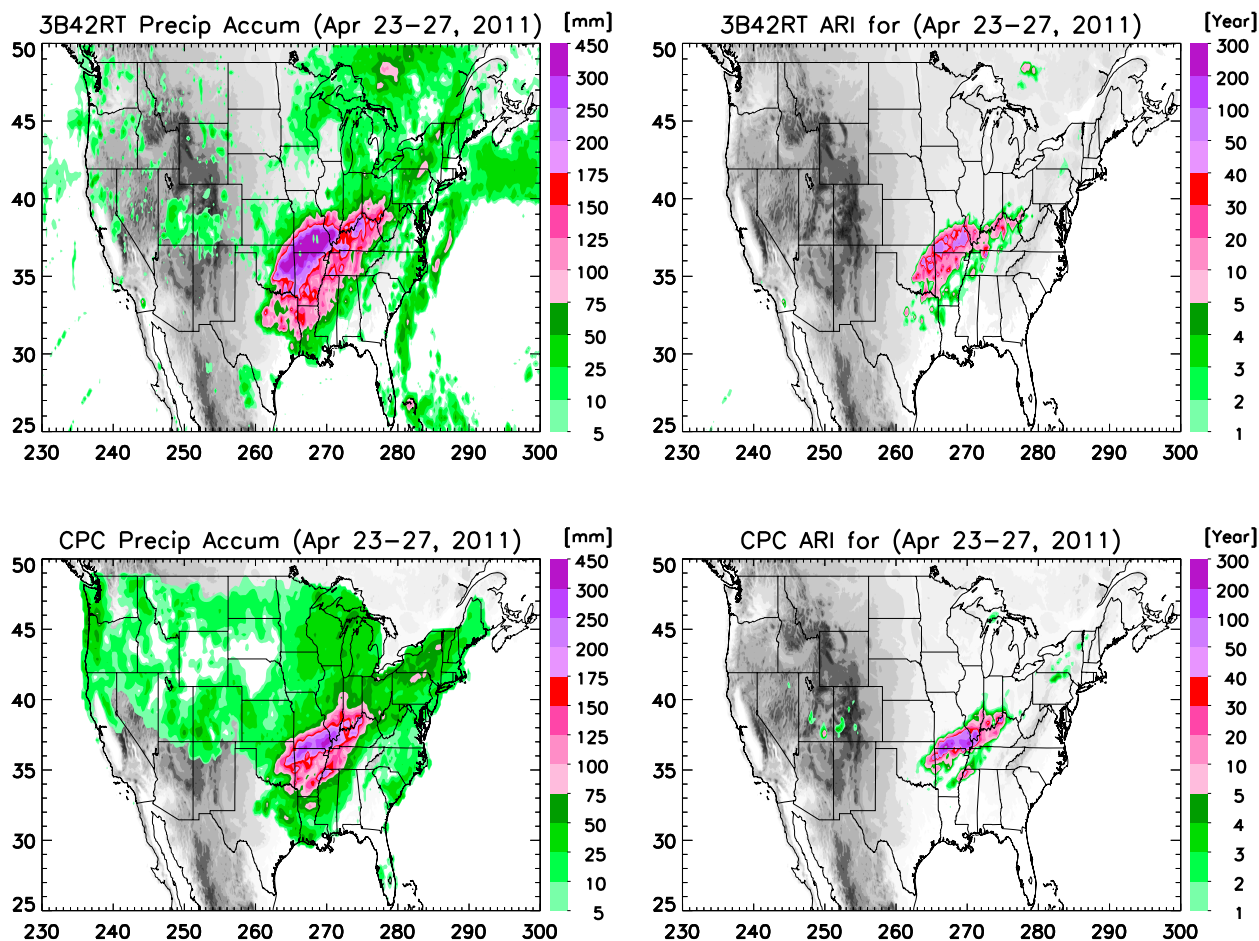


FIG. 10. (left) Precipitation accumulation (mm) and (right) corresponding ARI (yr) during 23–27 Apr 2011 from (top) 3B42RT data and (bottom) CPC daily unified precipitation data.

and extension of the extreme events with $\text{ARI} > 20$ –40 yr in the central United States, even though the ARI thresholds do not quite match the CPC threshold (Fig. 9). This is because the actual and climatological rains are subject to the same bias; the ARI value is less affected by the bias. We also note that the 3B42RT data produce few false alarms over the other regions of CONUS.

Complex orography still poses a significant challenge for satellite rainfall retrievals Huffman et al. (2014), so ARI computed from real-time measurements remains questionable in these areas. For example, the 3B42RT significantly underestimates the 7-day precipitation accumulations along the Colorado Front Range from Colorado Springs north to Fort Collins during 6–13 September 2013 that caused catastrophic flooding in the area (Gochis et al. 2015) (Fig. 11). The ARI map based on TMPA shows only a small area of elevated ARI, whereas the CPC data show a much larger area with ARI more than 50 years (also see Table 1). The

heavy precipitation in this event is a result of a slow-moving cold front clashing with warm humid monsoonal air from the south, but the 3B42RT failed to capture the low-level warm precipitation as the 3B42RT rainfall algorithm heavily relies on ice scattering signal over the land. As stated earlier, even the gauge-based CPC data may have large uncertainty because of sampling issues in mountainous areas. The user should be cautious when using satellite data for regions with complex orography. It is suggested that measurements other than precipitation, such as streamflow, be included in assessing hazard risks in these areas.

4. Conclusions

ARI maps can provide quantitative measures of the rarity of extreme precipitation events based on magnitude of observed rain rate and the rainfall climatology. They can be easily understood by the general public and decision makers. Near-real-time ARI maps can be

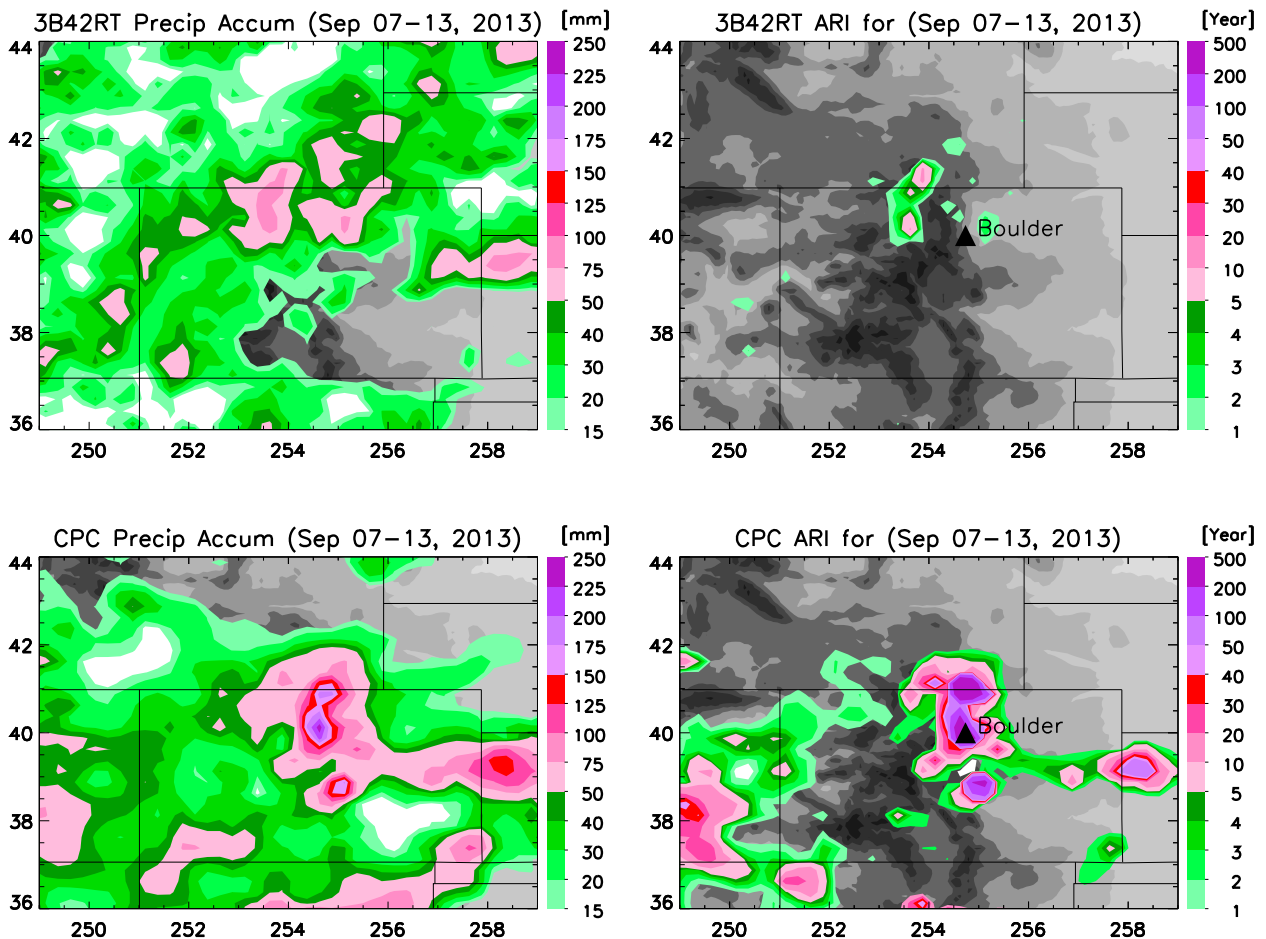


FIG. 11. (left) Precipitation accumulation (mm) and (right) corresponding ARI (yr) during 7–13 Sep 2013 from CPC daily unified precipitation data and 3B42RT data.

useful tools in assisting local planners in determining responses and allocating resources to ongoing rain events, either as short downpours or prolonged rain episodes. Previous detailed ARI maps could only be computed in regions with historical high-density rain gauge networks, such as in the United States, western Europe, China, and India. TRMM data make such maps possible over remote land regions and oceanic regions where rain gauge data are sparse or absent. We have generated ARI thresholds based on retrospective near-real-time TMPA data for 1–10-day rain accumulations using GEV distributions. Combining the near-real-time 3B42RT data and the ARI threshold tables, TRMM near-real-time precipitation data are mapped into return intervals for 1–10-day accumulations. This information provides a direct and quantitative measure of the severity of the rain events, which is useful in various weather and disaster monitoring applications.

There are a number of issues with the TRMM ARI product because of its short data record and the accuracy

of the real-time 3B42RT data. Large uncertainties exist in rainfall retrieval and computed ARI for regions with complex orography as shown by the Colorado case. The ARI estimates are generally quite uncertain for return years larger than 20. Therefore, unlike the NOAA Atlas 14, this product should not as yet be used as a reference for hydrometeorological and engineering design. Nevertheless, it can serve as an extreme precipitation warning system to provide useful warning information for potentially catastrophic events, even with the restrictions posed by a short data record and limited accuracy.

The system will undergo continuous improvement as the data record lengthens. As a continuing effort, we will test other approaches to enhance the statistical soundness of ARI computations. Specifically, we will test other distribution functions such as the generalized Pareto distribution for the peak-over-threshold method so more sample data can be incorporated into the computation (Leadbetter et al. 1983; Katz et al. 2002).

The maximum likelihood method used in current GEV fitting may not be the best approach, as a number of studies show that the probability weighted moment (L-moment) technique may produce better results for a short data record (Hosking 1990; Hosking and Wallis 1997; Katz et al. 2002; Gilleland and Katz 2006). In addition, regional statistics, rather than single grid statistics, will be incorporated to alleviate sporadic behavior in the short data record (Burn 1990; Hosking and Wallis 1997; Endreny and Imbeah 2009). The characteristics and uncertainty of satellite estimates of extreme precipitation, and the way these uncertainties propagate into ARI, will be further investigated.

With the launch of the Global Precipitation Measurement (GPM) mission (Hou et al. 2014), a new Integrated Multisatellite Retrievals for GPM (IMERG) will become available at an even higher resolution and accuracy (0.1° and 1 h; Huffman et al. 2014). The new GPM IMERG data will replace 3B42RT in the future with their increased capability for monitoring extreme precipitation events. As the TRMM–GPM data record length grows, these ARI products will be more robust and become increasingly important for research and hazard management.

Acknowledgments. This work is supported by the Precipitation Measuring Mission under Project NNX13AF73G (Headquarters Manager: Dr. R. Kakar), NASA Earth Science Division. The TMPA data are obtained from NASA Goddard Earth Sciences Data and Information Services Center (GES DISC): ftp://disc2.nascom.nasa.gov/data/TRMM/Gridded/Derived_Products/3B42RT/Daily/. We thank Dr. Siegfried Shubert's group for providing sample code for GEV calculation and three anonymous reviewers for providing many constructive suggestions.

REFERENCES

- Adhikari, P., Y. Hong, K. Douglas, D. Kirschbaum, J. Gourley, R. Adler, and G. Robert Brakenridge, 2010: A digitized global flood inventory (1998–2008): Compilation and preliminary results. *Nat. Hazards*, **55**, 405–422, doi:10.1007/s11069-010-9537-2.
- AghaKouchak, A., A. Behrangi, S. Sorooshian, K. Hsu, and E. Amitai, 2011: Evaluation of satellite-retrieved extreme precipitation rates across the central United States. *J. Geophys. Res.*, **116**, D02115, doi:10.1029/2010JD014741.
- Allan, R. P., and B. J. Soden, 2008: Atmospheric warming and the amplification of precipitation extremes. *Science*, **321**, 1481–1484, doi:10.1126/science.1160787.
- Ashley, S. T., and W. S. Ashley, 2008: Flood fatalities in the United States. *J. Appl. Meteor. Climatol.*, **47**, 806–818, doi:10.1175/2007JAMC1611.1.
- Bonnin, G. M., D. Martin, B. Lin, T. Parzybok, M. Yekta, and D. Riley, 2011: Semiarid southwest (Arizona, southeast California, Nevada, New Mexico, Utah). Precipitation-Frequency Atlas of the United States, Vol. 1, Version 5.0, NOAA Atlas 14, 271 pp. [Available online at http://www.nws.noaa.gov/oh/hdsc/PF_documents/Atlas14_Volume1.pdf.]
- Burn, D. H., 1990: Evaluation of regional flood frequency analysis with a region of influence approach. *Water Resour. Res.*, **26**, 2257–2265, doi:10.1029/WR026i010p02257.
- Chen, S., and Coauthors, 2013: Performance evaluation of radar and satellite rainfalls for Typhoon Morakot over Taiwan: Are remote-sensing products ready for gauge denial scenario of extreme events? *J. Hydrol.*, **506**, 4–13, doi:10.1016/j.jhydrol.2012.12.026.
- Cheng, L., A. AghaKouchak, E. Gilleland, and R. W. Katz, 2014: Non-stationary extreme value analysis in a changing climate. *Climatic Change*, **127**, 353–369, doi:10.1007/s10584-014-1254-5.
- Coles, S., 2001: *An Introduction to Statistical Modeling of Extreme Values*. Springer, 208 pp.
- Easterling, D. R., J. L. Evans, P. Ya. Groisman, T. R. Karl, K. E. Kunkel, and P. Ambenje, 2000: Observed variability and trends in extreme climate events: A brief review. *Bull. Amer. Meteor. Soc.*, **81**, 417–425, doi:10.1175/1520-0477(2000)081<0417:OVATIE>2.3.CO;2.
- Ebert, E. E., J. E. Janowiak, and C. Kidd, 2007: Comparison of near-real-time precipitation estimates from satellite observations and numerical models. *Bull. Amer. Meteor. Soc.*, **88**, 47–64, doi:10.1175/BAMS-88-1-47.
- Endreny, T. A., and N. E. A. Imbeah, 2009: Generating robust rainfall intensity-duration-frequency estimates with short-record satellite data. *J. Hydrol.*, **371** (1–4), 182–191, doi:10.1016/j.jhydrol.2009.03.027.
- Gilleland, E., and R. W. Katz, 2006: Analyzing seasonal to interannual extreme weather and climate variability with the extremes toolkit (extRemes). Preprints, *18th Conf. on Climate Variability and Change*, Atlanta, GA, Amer. Meteor. Soc., P2.15. [Available online at <https://ams.confex.com/ams/pdfpapers/101830.pdf>.]
- Gochis, D., and Coauthors, 2015: The Great Colorado Flood of September 2013. *Bull. Amer. Meteor. Soc.*, doi:10.1175/BAMS-D-13-00241.1, in press.
- Groisman, P. Ya., R. W. Knight, D. R. Easterling, T. R. Karl, G. C. Hegerl, and V. N. Razuvaev, 2005: Trends in intense precipitation in the climate record. *J. Climate*, **18**, 1326–1350, doi:10.1175/JCLI3339.1.
- Gruntfest, E., 2009: Editorial. *J. Flood Risk Manage.*, **2**, 83–84, doi:10.1111/j.1753-318X.2009.01028.x.
- Habib, E., A. Henschke, and R. F. Adler, 2009: Evaluation of TMPA satellite-based research and real-time rainfall estimates during six tropical-related heavy rainfall events over Louisiana, USA. *Atmos. Res.*, **94**, 373–388, doi:10.1016/j.atmosres.2009.06.015.
- Higgins, R. W., W. Shi, E. Yarosh, and R. Joyce, 2000: *Improved United States Precipitation Quality Control System and Analysis*. NCEP/Climate Prediction Center Atlas 7. [Available online at http://www.cpc.ncep.noaa.gov/products/outreach/research_papers/ncep_cpc_atlas/7/.]
- Hong, Y., R. F. Adler, A. Negri, and G. J. Huffman, 2007: Flood and landslide applications of near real-time satellite rainfall estimation. *Nat. Hazards*, **43**, 285–294, doi:10.1007/s11069-006-9106-x.
- , —, G. J. Huffman, H. Pierce, 2010: Applications of TRMM-based multi-satellite precipitation estimation for global runoff prediction: Prototyping a global flood modeling system. *Satellite Rainfall Applications for Surface Hydrology*, M. Gebremichael and F. Hossain, Eds., Springer, 245–265.

- Hosking, J. R. M., 1990: L-moments: Analysis and estimation of distributions using linear combinations of order statistics. *J. Roy. Stat. Soc.*, **52B**, 105–124.
- , and J. R. Wallis, 1997: *Regional Frequency Analysis: An Approach Based on L-Moments*. Cambridge University Press, 242 pp.
- Hossain, F., and D. P. Lettenmaier, 2006: Flood prediction in the future: Recognizing hydrologic issues in anticipation of the Global Precipitation Measurement mission. *Water Resour. Res.*, **42**, W11301, doi:10.1029/2006WR005202.
- Hou, A. Y., and Coauthors, 2014: The Global Precipitation Measurement mission. *Bull. Amer. Meteor. Soc.*, **95**, 701–722, doi:10.1175/BAMS-D-13-00164.1.
- Huffman, G. J., and Coauthors, 2007: The TRMM Multi-Satellite Precipitation Analysis (TMPA): Quasi-global, multiyear, combined sensor precipitation estimates at fine scales. *J. Hydrometeorol.*, **8**, 38–55, doi:10.1175/JHM560.1.
- , R. F. Adler, D. T. Bolvin, and E. Nelkin, 2010: The TRMM Multi-satellite Precipitation Analysis (TMPA). *Satellite Rainfall Applications for Surface Hydrology*, F. Hossain and M. Gebremichael, Eds., Springer Verlag, 3–22.
- , D. T. Bolvin, D. Braithwaite, K. Hsu, R. Joyce, and P. Xie, 2014: NASA Global Precipitation Measurement Integrated Multi-satellite Retrievals for GPM (IMERG). NASA Algorithm Theoretical Basis Doc. version 4.4, 30 pp. [Available online at http://pmm.nasa.gov/sites/default/files/document_files/IMERG_ATBD_V4.4.pdf.]
- Huntingford, C., R. G. Jones, C. Prudhomme, R. Lamb, H. C. Gash, and D. A. Jones, 2003: Regional climate-model predictions of extreme rainfall for a changing climate. *Quart. J. Roy. Meteor. Soc.*, **129**, 1607–1621, doi:10.1256/qj.02.97.
- IPCC, 2012: Summary for policymakers. *Managing the Risks of Extreme Events and Disasters to Advance Climate Change Adaptation*, C. B. Field et al., Eds., Cambridge University Press, 3–21.
- Katz, R. W., 2010: Statistics of extremes in climate change. *Climatic Change*, **100**, 71–76, doi:10.1007/s10584-010-9834-5.
- , M. B. Parlange, and P. Naveau, 2002: Statistics of extremes in hydrology. *Adv. Water Resour.*, **25**, 1287–1304, doi:10.1016/S0309-1708(02)00056-8.
- Kirschbaum, D., T. Stanley, and Y. Zhou, 2015: Spatial and temporal analysis of a global landslide catalog. *Geomorphology*, doi:10.1016/j.geomorph.2015.03.016, in press.
- Kotz, S., and S. Nadarajah, 2000: *Extreme Value Distributions: Theory and Applications*. Imperial College Press, 191 pp.
- Koutsoyiannis, D., and G. Baloutsos, 2000: Analysis of a long record of annual maximum rainfall in Athens, Greece, and design rainfall inferences. *Nat. Hazards*, **22**, 29–48, doi:10.1023/A:1008001312219.
- Lau, K.-M., and H.-T. Wu, 2007: Detecting trends in tropical rainfall characteristics, 1979–2003. *Int. J. Climatol.*, **27**, 979–988, doi:10.1002/joc.1454.
- Leadbetter, M. R., G. Lindren, and H. Rootzén, 1983: *Extremes and Related Properties of Random Sequences and Processes*. Springer, 336 pp.
- Li, L., and Coauthors, 2009: Evaluation of the real-time TRMM-based multi-satellite precipitation analysis for an operational flood prediction system in Nzoia Basin, Lake Victoria, Africa. *Nat. Hazards*, **50**, 109–123, doi:10.1007/s11069-008-9324-5.
- Liao, Z., Y. Hong, J. Wang, H. Fukuoka, K. Sassa, D. Karnawati, and F. Fathani, 2010: Prototyping an experimental early warning system for rainfall-induced landslides in Indonesia using satellite remote sensing and geospatial datasets. *Landslides*, **7**, 317–324, doi:10.1007/s10346-010-0219-7.
- Mehran, A., and A. AghaKouchak, 2014: Capabilities of satellite precipitation datasets to estimate heavy precipitation rates at different temporal accumulations. *Hydrol. Processes*, **28**, 2262–2270, doi:10.1002/hyp.9779.
- Min, S.-K., X. Zhang, F. W. Zwiers, and G. C. Hegerl, 2011: Human contribution to more-intense precipitation extremes. *Nature*, **470**, 378–381, doi:10.1038/nature09763.
- Parzybok, T., B. Clarke, and D. M. Hultstrand, 2011: Average recurrence interval of extreme rainfall in real-time. *Earthzine*. [Available online at <http://earthzine.org/2011/04/19/average-recurrence-interval-of-extreme-rainfall-in-real-time/>.]
- Perica, S., and Coauthors, 2013: Midwestern states (Colorado, Iowa, Kansas, Michigan, Minnesota, Missouri, Nebraska, North Dakota, Oklahoma, South Dakota, Wisconsin). *Precipitation-Frequency Atlas of the United States*, Vol. 8, Version 2.0, NOAA Atlas 14, 297 pp. [Available online at http://www.nws.noaa.gov/oh/hdsc/PF_documents/Atlas14_Volume8.pdf.]
- Schubert, S. D., Y. Chang, M. J. Suarez, and P. J. Pegion, 2008: ENSO and wintertime extreme precipitation events over the contiguous United States. *J. Climate*, **21**, 22–39, doi:10.1175/2007JCLI1705.1.
- Shen, Y., A. Xiong, Y. Wang, and P. Xie, 2010: Performance of high-resolution satellite precipitation products over China. *J. Geophys. Res.*, **115**, D02114, doi:10.1029/2009JD012097.
- Smith, K., and R. Ward, 1998: *Floods: Physical Processes and Human Impacts*. John Wiley and Sons, 394 pp.
- Sorooshian, S., and Coauthors, 2011: Advanced concepts on remote sensing of precipitation at multiple scales. *Bull. Amer. Meteor. Soc.*, **92**, 1353–1357, doi:10.1175/2011BAMS3158.1.
- Stampoulis, D., and E. N. Anagnostou, 2012: Evaluation of global satellite rainfall products over continental Europe. *J. Hydrometeorol.*, **13**, 588–603, doi:10.1175/JHM-D-11-086.1.
- Su, F. G., Y. Hong, and D. P. Lettenmaier, 2008: Evaluation of TRMM Multisatellite Precipitation Analysis (TMPA) and its utility in hydrologic prediction in La Plata basin. *J. Hydrometeorol.*, **9**, 622–640, doi:10.1175/2007JHM944.1.
- , H. Gao, G. J. Huffman, and D. P. Lettenmaier, 2011: Potential utility of the real-time TMPA-RT precipitation estimates in streamflow prediction. *J. Hydrometeorol.*, **12**, 444–455, doi:10.1175/2010JHM1353.1.
- Tian, Y., C. D. Peters-Lidard, B. J. Choudhury, and M. Garcia, 2007: Multitemporal analysis of TRMM-based satellite precipitation products for land data assimilation applications. *J. Hydrometeorol.*, **8**, 1165–1183, doi:10.1175/2007JHM859.1.
- , and Coauthors, 2009: Component analysis of errors in satellite-based precipitation estimates. *J. Geophys. Res.*, **114**, D24101, doi:10.1029/2009JD011949.
- Towler, E., and Coauthors, 2010: Modeling hydrologic and water quality extremes in a changing climate: A statistical approach based on extreme value theory. *Water Resour. Res.*, **46**, W11504, doi:10.1029/2009WR008876.
- Trenberth, K. E., A. Dai, R. M. Rasmussen, and D. B. Parsons, 2003: The changing character of precipitation. *Bull. Amer. Meteor. Soc.*, **84**, 1205–1217, doi:10.1175/BAMS-84-9-1205.
- U.S. Department of the Interior Bureau of Reclamation, 1987: Design of small dams. 3rd ed. U.S. Government Printing Office Water Resources Tech. Publ., 860 pp. [Available online at http://www.usbr.gov/pmts/hydraulics_lab/pubs/manuals/SmallDams.pdf.]
- Villarini, G., 2010: Evaluation of the research-version TMPA rainfall estimate at its finest spatial and temporal scales over the Rome metropolitan area. *J. Appl. Meteor. Climatol.*, **49**, 2591–2602, doi:10.1175/2010JAMC2462.1.

- , and W. F. Krajewski, 2007: Evaluation of the research version TMPA three-hourly $0.25^{\circ} \times 0.25^{\circ}$ rainfall estimates over Oklahoma. *Geophys. Res. Lett.*, **34**, L05402, doi:[10.1029/2006GL029147](https://doi.org/10.1029/2006GL029147).
- Wang, J., and Coauthors, 2011: The coupled routing and excess storage (CREST) distributed hydrological model. *Hydrol. Sci. J.*, **56**, 84–98, doi:[10.1080/02626667.2010.543087](https://doi.org/10.1080/02626667.2010.543087).
- Wilks, D. S., 2011: *Statistical Methods in the Atmospheric Sciences*. 3rd ed. Academic Press, 704 pp.
- Wu, H., R. F. Adler, Y. Hong, Y. Tian, and F. Policelli, 2012: Evaluation of global flood detection using satellite-based rainfall and a hydrologic model. *J. Hydrometeor.*, **13**, 1268–1284, doi:[10.1175/JHM-D-11-087.1](https://doi.org/10.1175/JHM-D-11-087.1).
- Yatagai, A., K. Kamiguchi, O. Arakawa, A. Hamada, N. Yasutomi, and A. Kitoh, 2012: APHRODITE: Constructing a long-term daily gridded precipitation dataset for Asia based on a dense network of rain gauges. *Bull. Amer. Meteor. Soc.*, **93**, 1401–1415, doi:[10.1175/BAMS-D-11-00122.1](https://doi.org/10.1175/BAMS-D-11-00122.1).
- Yilmaz, K. K., R. F. Adler, Y. Tian, Y. Hong, and H. F. Pierce, 2010: Evaluation of a satellite-based global flood monitoring system. *Int. J. Remote Sens.*, **31**, 3763–3782, doi:[10.1080/01431161.2010.483489](https://doi.org/10.1080/01431161.2010.483489).